Weak-coupling approximations in non-Markovian transport

Philipp Zedler,* Gernot Schaller, Gerold Kiesslich, Clive Emary, and Tobias Brandes
Technische Universität Berlin, Hardenbergstrasse 36, 10623 Berlin, Germany

(Received 12 February 2009; revised manuscript received 13 May 2009; published 14 July 2009)

We study the transport properties of the Fano-Anderson model with non-Markovian effects, which are introduced by making one tunneling-rate energy dependent. We show that the non-Markovian master equation may fail if these effects are strong. We evaluate the stationary current, the zero-frequency current noise, and the occupation dynamics of the resonant level by means of a quantum master-equation approach within different approximation schemes and compare the results to the exact solution obtained by the scattering theory and Green's functions.

DOI: 10.1103/PhysRevB.80.045309 PACS number(s): 72.10.Bg, 03.65.Nk, 05.60.Gg

I. INTRODUCTION

The ongoing progress in measuring tiny fluctuations of charge currents through nanoscale conductors[1–3] has led to an increased theoretical interest in non-Markovian effects revealed in such experiments.[4,5] Of particular interest are the non-Markovian dynamics induced by the coupling to fermionic[6,7] and/or bosonic[8–10] environments and their influence on steady-state transport observables such as the cumulants of the stochastic charge-transfer process.[11] Our present work focuses on such effects due to the coupling to electronic reservoirs.

There exist various techniques for describing open quantum systems coupled to fermionic reservoirs, e.g., the scattering theory and Green's functions,[12–14] or quantum master equations starting from the von Neumann equation for the total density operator[15] or the Wigner-Boltzmann approach.[16–18] Master equations are widely considered with a conductor-lead coupling in Born-Markov approximation (see, e.g., Refs. 19–21), which is only strictly valid for weak coupling and constant contact density of states in the energy range of interest. Consequently, to explore effects beyond the common Born-Markov approximation, one would study higher-order perturbation theory in the contact coupling (e.g., Refs. 22–24) and/or allow for energy-dependent tunneling rates, i.e., go beyond the wideband approximation.[14,25–29] In this work, we choose the latter while analyzing perturbative approaches in lowest-order tunnel coupling only. In particular, we address the question in which limits it is possible to describe non-Markovian physics with master equations.

A conceptionally simple model for this purpose consists of a single resonant level (e.g., the ground state of a quantum dot or a molecule) weakly coupled to two electronic leads in equilibrium and a Lorentzian-shaped density of states for one of the leads. This model is equivalent to two serially coupled quantum dots[9] and can be interpreted as a quantum dot coupled to a reservoir with finite electron relaxation time.

To enable an exact solution and for the sake of simplicity, we neglect Coulomb interaction and, consequently, prominent effects such as Coulomb blockade or Kondo correlations. This, of course, constrains the use of our results for quantitative understandings of transport experiments. Our aim, however, is a comparison of different approximation schemes for master equations in an electronic transport problem that has an exact solution.

We will show that the non-Markovian master equation (NMME) in the wideband limit produces reasonable results for the current and noise. However, reducing the bandwidth yields qualitative and quantitative deviations—even the emergence of unphysical results such as negative Fano factors. The exact time evolution of the resonant-level occupation can only be obtained by the NMME in the wideband limit where even a Markovian master equation covers the exact dynamics. In the short-time limit, the NMME result well approximates the exact evolution regardless of the bandwith. However, for very small bandwidths, the NMME generates negative unphysical probabilities. We demonstrate how this can be avoided by a dynamical-coarse-graining method.

The paper is organized as follows. In Secs. II A and II B, we introduce the model and provide the known exact solution obtained by the scattering theory and Green's functions. In Sec. II C, the equivalence to the double-dot model is discussed. In Sec. III A, we introduce the non-Markovian master equation and, in Sec. III B, the dynamical-coarse-graining approach. In Sec. IV, the steady-state current and the Fano factor are compared to the exact and NMME solution. Finally, the occupation dynamics of the resonant level is discussed.

II. MODEL

A. Hamiltonian

We start from the well-known single resonant-level model,[14,30–34] that is described by a Hamiltonian where tunneling between two leads can be realized via a localized quantum-dot state,

$$H = \epsilon_d d^\dagger d + \sum_{k,a} \epsilon_{ka} c_{ka}^\dagger c_{ka} + \sum_{k,a} (t_{ka} d^\dagger c_{ka} + \text{H.c.}). \quad (1)$$

The fermionic operators $d/d^\dagger$ annihilate/create an electron on the dot and $c_{ka}/c_{ka}^\dagger$ annihilate/create an electron in lead $a \in \{R,L\}$ with momentum k. We choose a Lorentzian-shaped right tunneling rate, such as in Refs. 25 and 26,

$$\Gamma_R(\omega) = \frac{\Gamma_{R,0}^2}{\pi} \frac{\delta_R}{(\omega - \varepsilon_R)^2 + \delta_R^2}, \quad (2)$$

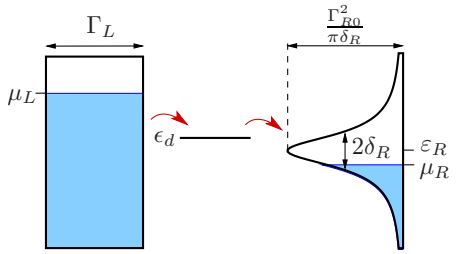

FIG. 1. (Color online) Single resonant level coupled to two leads with one constant and one Lorentzian tunneling rate. In the infinite-bias limit, $\mu_L \to \infty$ and $\mu_R \to -\infty$.

and a flat left tunneling rate Γ_L, both related to the microscopic parameters via $\Gamma_a(\omega)=2\pi\Sigma_k|t_{ka}|^2\delta(\omega-\epsilon_{ka})$. A sketch of the model is given in Fig. 1. We work in the infinite-bias limit, where we couple the left and right leads to two particle reservoirs in a way that the left lead is completely occupied and the right lead is completely empty, i.e., $\mu_L \to \infty$ and $\mu_R \to -\infty$, such that the left Fermi function takes the value 1 and the right one takes the value 0.

The retarded and advanced self-energies of our model are evaluated exactly[14,32,34] as

$$\Sigma^{R/A}(\omega)=\sum_{k,a}\frac{|t_{ka}|^2}{\omega-\epsilon_{ka}\pm i0^+}=\Lambda(\omega)\mp i\frac{\Gamma(\omega)}{2}. \tag{3}$$

The imaginary part $\Gamma(\omega)=\Gamma_L(\omega)+\Gamma_R(\omega)$ is connected to the inverse lifetime whereas the real part

$$\Lambda(\omega)=\frac{1}{2\pi}\mathcal{P}\int_{-\infty}^{\infty}d\omega'\frac{\Gamma(\omega')}{\omega-\omega'} \tag{4}$$

(where $\mathcal{P}$ denotes the principal value) induces a level shift which is fully determined by the tunneling rate (Kramers-Kronig relation). It will turn out that all quantities concerning transport statistics and the occupation of the quantum dot can be expressed in terms of $\Gamma_a(\omega)$ and ϵ_d only.

B. Exact solution

To evaluate transport quantities, we need the transmission coefficient,[35]

$$T(\omega)=\frac{\Gamma_L(\omega)\Gamma_R(\omega)}{|\omega-\epsilon_d-\Sigma^R(\omega)|^2}, \tag{5}$$

which is related to the dot-spectral function $A(\omega) := i[G^R(\omega)-G^A(\omega)]$ via $T(\omega)=\frac{\Gamma_L(\omega)\Gamma_R(\omega)}{\Gamma(\omega)}A(\omega)$. Scattering theory[1] then yields the current I and the zero-frequency noise S which at infinite bias are

$$I=e\int_{-\infty}^{\infty}\frac{d\omega}{2\pi}T(\omega),$$

$$S=e^2\int_{-\infty}^{\infty}\frac{d\omega}{2\pi}T(\omega)[1-T(\omega)], \tag{6}$$

where e is the elementary charge (chosen negative). The time-dependent occupation probability $n_d(t)$ can be expressed with the Green's functions.[36,37] We use that at infinite bias, the left Fermi function is unity and the right is zero. For simplicity, we assume $n_d(0)=0$ and thus

$$n_d(t)=-i\sum_k G^R_{d,kL}(t)iG^A_{kL,d}(-t)=\sum_k|G^R_{d,kL}(t)|^2, \tag{7}$$

where we have used $G^A_{ka,d}(-t)=[G^R_{d,ka}(t)]^*$.

The required Green's functions are obtained using equations of motion[14,32–34] and read as

$$G^R_{d,kL}(t)=t_{kL}\int_{-\infty}^{\infty}\frac{d\omega}{2\pi}\frac{1}{\omega-\epsilon_{kL}+i0^+}\frac{e^{-i\omega t}}{\omega-\epsilon_d-\Sigma^R(\omega)}, \tag{8}$$

which, upon inserting $1=\int_{-\infty}^{\infty}\delta(\omega-\epsilon_{kL})d\omega$, yields the explicit result

$$n_d(t)=\int_{-\infty}^{\infty}\frac{d\omega}{2\pi}\Gamma_L\left|\int_{-\infty}^{\infty}\frac{d\omega'}{2\pi}\frac{1}{\omega'-\omega+i0^+}\frac{e^{-i\omega' t}}{\omega'-\epsilon_d-\Sigma^R(\omega')}\right|^2. \tag{9}$$

This can alternatively be obtained from a direct calculation without the Green's functions.[38]

For the Lorentzian-shaped right tunneling rate (2), the Kramers-Kronig relation (4) yields the level-shift function,

$$\Lambda(\omega)=\frac{\Gamma_{R,0}^2}{2\pi}\frac{\omega-\varepsilon_R}{(\omega-\varepsilon_R)^2+\delta_R^2}, \tag{10}$$

and the self energy (3) can be simplified to

$$\Sigma^{R/A}(\omega)=\mp i\frac{\Gamma_L}{2}+\frac{\Gamma_{R,0}^2}{2\pi}\frac{1}{\omega-\varepsilon_R\pm i\delta_R}. \tag{11}$$

With Lorentzian-shaped tunneling rates, we can analytically integrate the expressions for current and noise (6) and, with the abbreviations $\bar{\Gamma} := \Gamma_L+2\delta_R$ and $\epsilon := \epsilon_d-\varepsilon_R$, we obtain

$$I=e\frac{2\Gamma_L\delta_R\bar{\Gamma}\Gamma_{R,0}^2/\pi}{(\Gamma_L\delta_R+\Gamma_{R,0}^2/\pi)\bar{\Gamma}^2+4\epsilon^2\Gamma_L\delta_R},$$

$$S=Ie\left(1-\frac{2\Gamma_L\delta_R\Gamma_{R,0}^2}{\pi\bar{\Gamma}}\frac{4\epsilon^2(\Gamma_L^3+8\delta_R^3)+\bar{\Gamma}^3(\bar{\Gamma}^2+2\Gamma_L\delta_R+2\Gamma_{R,0}^2/\pi)}{[(\Gamma_L\delta_R+\Gamma_{R,0}^2/\pi)\bar{\Gamma}^2+4\epsilon^2\Gamma_L\delta_R]^2}\right). \tag{12}$$

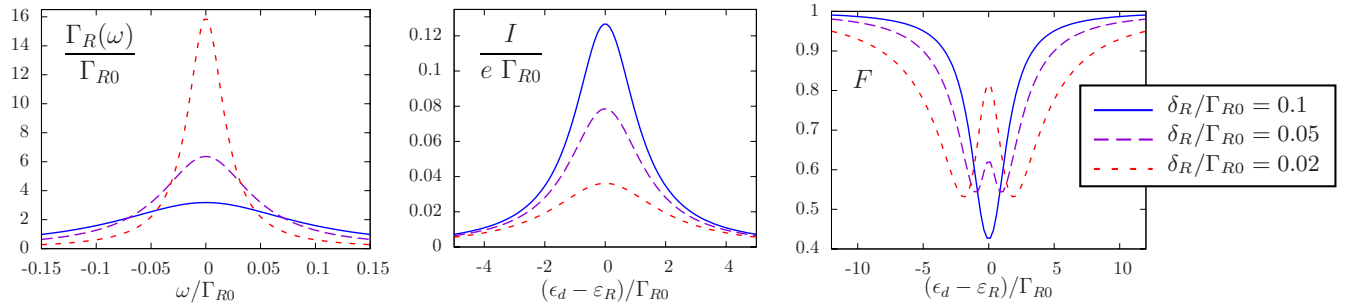

FIG. 2. (Color online) The left plot shows the right tunneling rate $\Gamma_R(\omega)$ as a function of the energy ω. We further show how the current I and Fano factor F behave as a function of the detuning $\epsilon_d-\varepsilon_R$. The bandwidth δ_R takes the three values shown on the right. For all curves, we have $\Gamma_L=\Gamma_{R,0}$. Results from the exact Green's functions.

C. Comparison with double-dot model

Our model has an exact correspondence with an effective wideband two-level Fano-Anderson model[25] with Hamiltonian

$$\bar{H}=\bar{\epsilon}_L d_L^\dagger d_L+\bar{\epsilon}_R d_R^\dagger d_R+\bar{T}_C d_L^\dagger d_R+\bar{T}_C^* d_R^\dagger d_L+\sum_{k,a}\bar{\epsilon}_{ka}c_{ka}^\dagger c_{ka}+\sum_{k,a}(\bar{t}_{ka}d_a^\dagger c_{ka}+\text{H.c.}),\tag{13}$$

with a left and a right dot state d_L and d_R and a coupling $\bar{T}_C$ between them. Each lead couples only to its adjacent dot. The transmission probability is[39]

$$\bar{T}(\omega)=\frac{\bar{\Gamma}_L\bar{\Gamma}_R|\bar{T}_C|^2}{\left|(\omega-\bar{\epsilon}_L+i\bar{\Gamma}_L/2)(\omega-\bar{\epsilon}_R+i\bar{\Gamma}_R/2)-|\bar{T}_C|^2\right|^2}.\tag{14}$$

Comparison to Eq. (5), with appropriate $\Gamma_R(\omega)$ and $\Lambda(\omega)$, reveals the exact mapping $\bar{T}(\omega)=T(\omega)$ by the correspondence

$$\bar{\Gamma}_L\leftrightarrow\Gamma_L,$$

$$|\bar{T}_C|^2\leftrightarrow\Gamma_{R,0}^2/(2\pi),$$

$$\bar{\Gamma}_R\leftrightarrow 2\delta_R,$$

$$\bar{\epsilon}_L\leftrightarrow\epsilon_d,$$

$$\bar{\epsilon}_R\leftrightarrow\varepsilon_R.\tag{15}$$

Since the cumulant generating function can be expressed solely in terms of the transmission probabilities,[1,40,41] not only the first two cumulants[42] but *all* current cumulants of the two models coincide.

When we plot current and Fano factor $F=S/(Ie)$ as a function of the detuning $\epsilon_d-\varepsilon_R$ in Fig. 2, we find the typical structures of the corresponding quantities for the noninteracting double quantum dot:[42,43] the current exhibits a maximum when the detuning vanishes. For the noise, we find a minimum in resonance for broad tunneling rates, when δ_R becomes sufficiently small a new maximum in the Fano factor at resonance grows out of the minimum.

III. NON-MARKOVIAN DYNAMICS

A. Non-Markovian master equation

To treat non-Markovian effects in a transport master-equation framework, one writes the master equation as an integro-differential equation for the n-resolved reduced density matrix

$$\dot{\rho}_n(t)=\sum_{n'}\int_0^t\mathcal{W}_{n-n'}(t-t')\rho_{n'}(t')dt',\tag{16}$$

where n denotes the number of charges that have crossed the considered system. In Appendix A, we show how our system can be described with such an equation using the Born approximation. All $\mathcal{W}_n(t)$ vanish except when $n=0$ or $n=1$, where we find

$$\mathcal{W}_0(t)=\begin{pmatrix}-\gamma_L(t) & 0\\ \gamma_L(t) & -\gamma_R(t)\end{pmatrix},$$

$$\mathcal{W}_1(t)=\begin{pmatrix}0 & \gamma_R(t)\\ 0 & 0\end{pmatrix}\tag{17}$$

with

$$\gamma_R(t)=2\int\frac{d\omega}{2\pi}\Gamma_R(\omega)\cos[(\omega-\epsilon_d)t]=\frac{\Gamma_{R,0}^2}{\pi}e^{-\delta_R t}\cos[(\varepsilon_R-\epsilon_d)t],$$

$$\gamma_L(t)=2\int\frac{d\omega}{2\pi}\Gamma_L\cos[(\omega-\epsilon_d)t]=2\Gamma_L\delta(t).\tag{18}$$

We proceed with performing a Fourier summation and a Laplace transform via

$$\hat{\mathcal{W}}(\chi,z)\equiv\sum_n e^{in\chi}\int_0^\infty e^{-zt}\mathcal{W}_n(t)dt=\hat{\mathcal{W}}_0(z)+\hat{\mathcal{W}}_1(z)e^{i\chi}=\begin{pmatrix}-\hat{\gamma}_L(z) & e^{i\chi}\hat{\gamma}_R(z)\\ \hat{\gamma}_L(z) & -\hat{\gamma}_R(z)\end{pmatrix},\tag{19}$$

where

$$\hat{\gamma}_R(z) = \frac{\Gamma_{R,0}^2}{\pi} \frac{z+\delta_R}{(z+\delta_R)^2+(\varepsilon_R-\epsilon_d)^2},$$

$$\hat{\gamma}_L(z) = \Gamma_L. \tag{20}$$

We will use the abbreviation $\hat{\gamma}(z)=\hat{\gamma}_L(z)+\hat{\gamma}_R(z)$. In order to avoid the tedious inverse Laplace transform, we can use a recently developed elegant method to evaluate current and noise.[11,44] As it has only applied a few times until now,[11,44–46] we show the explicit calculation for our model in Appendix B and obtain the following formulae:

$$I = e\frac{\hat{\gamma}_L(0)\hat{\gamma}_R(0)}{\hat{\gamma}(0)},$$

$$S = Ie\left\{\frac{\hat{\gamma}_R^2(0)}{\hat{\gamma}^2(0)}[1+2\hat{\gamma}_L'(0)]+\frac{\hat{\gamma}_L^2(0)}{\hat{\gamma}^2(0)}[1+2\hat{\gamma}_R'(0)]\right\}. \tag{21}$$

We easily obtain the occupation of the dot by evaluating the density matrix in Laplace space $\hat{\rho}(z)=[z-\hat{\mathcal{W}}(z)]^{-1}\rho(t=0)$. To obtain the time-resolved dynamics, one has to perform the inverse Laplace transform (Bromwich integral) by collecting all the corresponding residues.

B. Markovian master equation

A Markovian master equation (MME) follows from Eq. (16) by the integration $\mathcal{L}_n=\int_0^\infty \mathcal{W}_n(t)dt=\hat{\mathcal{W}}_n(z=0)$ and leads to

$$\mathcal{L}_0 = \begin{pmatrix} -\Gamma_L & 0 \\ \Gamma_L & -\Gamma_R(\epsilon_d) \end{pmatrix}, \quad \mathcal{L}_1 = \begin{pmatrix} 0 & \Gamma_R(\epsilon_d) \\ 0 & 0 \end{pmatrix}. \tag{22}$$

When we use this to evaluate noise, we end up with the same result as in Eq. (21) but without the derivatives $\hat{\gamma}_L'(0)$ and $\hat{\gamma}_R'(0)$. For the equilibrium density matrix, we find $\rho_{00}(t=\infty)=\Gamma_R(\epsilon_d)/[\Gamma_L+\Gamma_R(\epsilon_d)]$, which is identical with the NMME result. The advantage of the additional Markov approximation is that the positivity of the density matrix will be conserved as one obtains a Lindblad-type master equation.[47] The disadvantage is that some information about the shape of the tunneling rates is lost.

C. Dynamical coarse graining

A second approach to quantum transport is the recently developed dynamical-coarse-graining (DCG) method.[48] The coarse-graining method is also a second-order weak-coupling approximation, although it can be extended to higher orders. Instead of solving a single master equation, it solves a continuous set $\dot{\rho}^\tau(t)=\mathcal{L}^\tau\rho^\tau(t)$ and then interpolates through the solutions $\rho^\tau(t)=e^{\mathcal{L}^\tau t}\rho_0$ at $t=\tau$. The coarse-grained Liouvillian can be derived[48] by matching the second-order expansion of the formal solution in the interaction picture $\tilde{\chi}(t)=\tilde{U}(t)\chi(0)\tilde{U}^\dagger(t)$ [where $\tilde{U}(t)=T\exp\{-i\int_0^t H_{SB}(t')dt'\}$ with the time-ordering operator T] with the second-order expansion of $\rho^\tau(t)=e^{\mathcal{L}^\tau t}\rho^\tau(0)$ at time $t=\tau$. For our specific model, following Ref. 38, we obtain

$$\mathcal{L}^\tau = \int_{-\infty}^{\infty}\frac{d\omega}{2\pi}\tau\,\mathrm{sinc}^2\left(\frac{(\omega-\epsilon_d)\tau}{2}\right)\begin{pmatrix} -\Gamma_L(\omega) & \Gamma_R(\omega) \\ \Gamma_L(\omega) & -\Gamma_R(\omega) \end{pmatrix}, \tag{23}$$

where $\mathrm{sinc}\,x\equiv\frac{\sin x}{x}$. The coarse-graining method combines the two advantages of the Born and the Born-Markov approximation. For finite times, it is sensitive to the shape of the tunneling rates and at the same time it preserves positivity since the $\mathcal{L}^\tau$ are of Lindblad form. Due to the identity $\lim_{\tau\to\infty}\tau\mathrm{sinc}^2[\frac{(\omega-\epsilon_d)\tau}{2}]=2\pi\delta(\omega-\epsilon_d)$, we see that for large times the coarse-graining method yields the same steady-state density matrix as the two other approximations. Also for the current and Fano factor, we have reproduced the results of the MME. In contrast to fixed graining-time derivations of master equations,[7,49] DCG dynamically adapts the coarse-graining time with the physical time, which in the long-time limit yields the Born-Markov secular approximation. Both approaches yield completely positive maps but may lead to different stationary states.

IV. DISCUSSION

A. Current

To get a first idea of the difference between the exact solution and the NMME, it is instructive to take a look at the stationary current I. The stationary current is not sensitive to non-Markovian effects[11] since it only depends on the steady-state occupation, and thus all three presented approximations coincide. The two plots in Fig. 3 show the current as a function of the width of the right tunneling rate δ_R. We observe that for large δ_R (Markovian limit), the master equations meet the exact solution very well while for small δ_R enormous deviations occur. In the absence of detuning $\epsilon_d-\varepsilon_R=0$, the master equations overestimate the current, but they underestimate it for sufficiently large detuning. As an inset in Fig. 3, we choose the value $\delta_R/\Gamma_{R,0}=0.1$ and show how the spectral function of the dot state $A(\omega)$, the right tunneling rate $\Gamma_R(\omega)$ and the transmission coefficient $T(\omega)$ behave there.

Without detuning, the spectral function exhibits a minimum at energies where the tunneling rate is maximal. Thus, the true quantum-mechanical transmission is smaller than the master-equation result, which depends exclusively on the value of the tunneling rate at the dot level $\Gamma_R(\epsilon_d)$. This leads to the underestimation of the current by the master equations when detuning is present because $\Gamma_R(\epsilon_d)$ is very small then. The exact result, by contrast, takes into account that the spectral function exhibits a small side peak near the maximum of $\Gamma_R(\omega)$ that enhances the probability for tunneling.

B. Fano factor

In Fig. 4, we show results for the Fano factor $F=S/(Ie)$ (exact, with NMME and with MME or DCG). When the condition

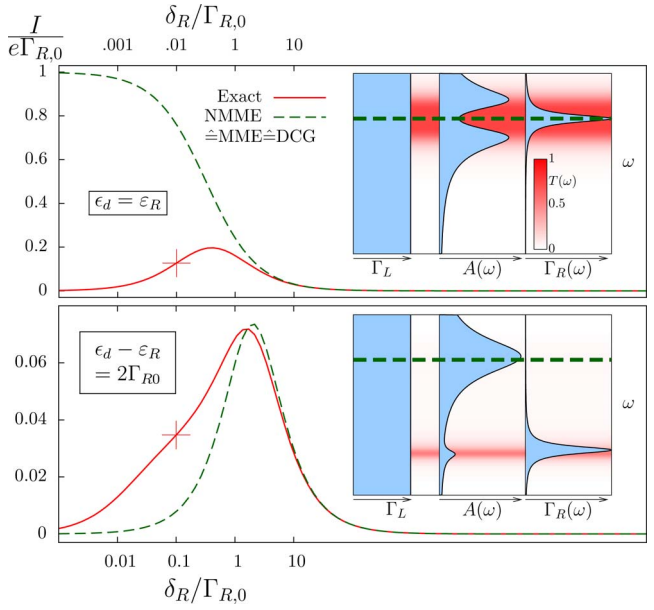

FIG. 3. (Color online) Current I as a function of the width δ_R on a logarithmic scale in absence (upper part) and presence (lower part) of detuning, exact (red and solid) and with the NMME ≙ MME ≙ DCG (green and dashed) with the parameters $\Gamma_L=\Gamma_{R,0}$. Inset: for the marked points at $\delta_R/\Gamma_{R,0}=0.1$, we plot as functions of ω the left tunneling rate Γ_L, the dot-spectral function $A(\omega)$, and the right tunneling rate $\Gamma_R(\omega)$, with a density plot of the transmission probability $T(\omega)$ in the background. The dashed green line marks the level of the dot state. The master equations depend only on $\Gamma_R(\epsilon_d)$ while the exact solution is sensitive to the detailed shape of $A(\omega)$ and $T(\omega)$.

$$\frac{\delta_R}{\Gamma_{R,0}} \gg 1 \tag{24}$$

is fulfilled, all formalisms agree. Furthermore, for constant tunneling rates, the NMME yields the Markovian result $F=\frac{\Gamma_L^2+\Gamma_R^2(\epsilon_d)}{[\Gamma_L+\Gamma_R(\epsilon_d)]^2}$.

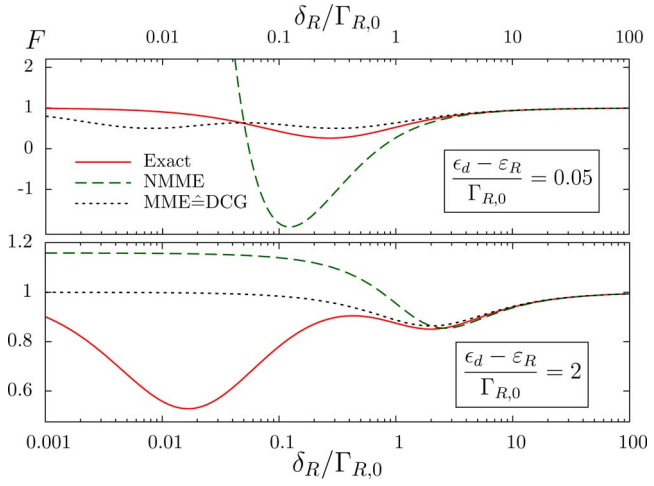

FIG. 4. (Color online) Fano factor F as a function of the width δ_R on a logarithmic scale. Parameters are $\Gamma_L=\Gamma_{R,0}$ and the detunings $\epsilon_d-\varepsilon_R$ indicated in each plot.

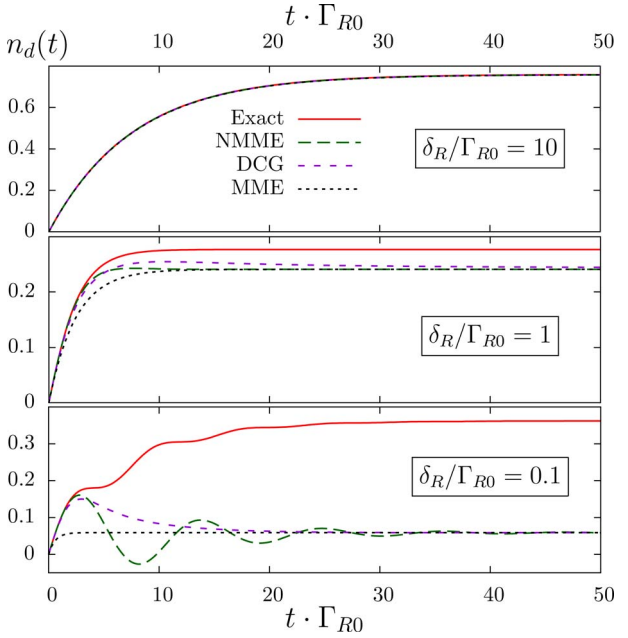

FIG. 5. (Color online) Time-dependent occupation probability $n_d(t)$, exact solution, and solution in the three presented approximations parameters are $\epsilon_d=\Gamma_{R,0}$ and $\epsilon_d-\epsilon_R=\Gamma_L=0.1\Gamma_{R,0}$. The width δ_R takes the values denoted in each plot.

The exact Fano factor shows one minimum for small detuning and two minima for large detuning, which originates from the double-peak structure of the spectral function shown in Fig. 3. However, there is no simple quantitative connection between the locations of the extrema in the Fano factor and in the spectral function. This is similar to the Fano factor as a function of the detuning in Fig. 2, where for small width δ_R a second minimum appears, that is, again not connected to the spectral function's properties in a simple way.

The NMME reproduces one of the two minima, but not both, and it produces super-Poissonian noise, where it should not appear. If the detuning $\epsilon_d-\varepsilon_R$ becomes very small, the NMME even overestimates the minimum so strongly that it yields an unphysical negative Fano factor.

The MME is not everywhere close to the exact result but it is, on average, closer than the NMME result and per construction yields physical results (Lindblad form). For the DCG method, we have found that it yields the same result as the MME.

C. Time-resolved occupation probabilities

One key advantage of the DCG approach results from its ability to preserve positivity and at the same time to be more sensitive to the shape of the tunneling rates than the MME.[48] We therefore evaluate the time-dependent occupation probability of the localized level with four different methods: exact, with the NMME, with the MME, and with DCG. In Fig. 5, we find that at sufficiently wide bands, i.e., $\delta_R \geq \Gamma_{R,0}$, all three approximations meet the exact result very well.

For smaller δ_R, one recognizes that in the stationary limit, the three approximations coincide with each other but not

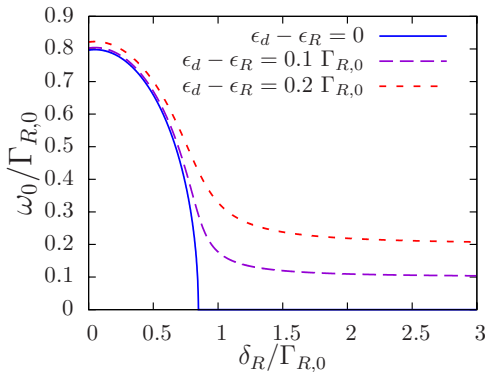

FIG. 6. (Color online) Frequency ω_0 as a function of the detuning $\omega_d - \omega_R$ for the parameters $\Gamma_L = 0.1\Gamma_{R,0}$ and $\epsilon_d = \Gamma_{R,0}$.

with the exact solution. The most prominent features of the exact occupation $n_d(t)$ are oscillations as a function of time t. The NMME approximation captures the oscillations as non-Markovian features of the reservoirs, as it should but it strongly overestimates them. If the steady state is sufficiently close to zero, the NMME can lead to negative occupation probabilities, such as in the third plot.

In order to better understand the exact result, we explicitly perform the two integrations in Eq. (9), which leads to

$$\begin{aligned} n_d(t) = {} & \Gamma_L \frac{\delta_R(\bar{\Gamma}^2 + 4\epsilon^2) + \bar{\Gamma}\Gamma_{R,0}^2/\pi}{\delta_R(\bar{\Gamma}^2 + 4\epsilon^2) + \bar{\Gamma}^2\Gamma_{R,0}^2/\pi} \\ & + i\Gamma_L \frac{(\omega_1 - \epsilon_R + i\delta_R)(\omega_1^* - \epsilon_R - i\delta_R)}{(\omega_1 - \omega_2)(\omega_1^* - \omega_2^*)(\omega_1 - \omega_1^*)} e^{i(\omega_1^* - \omega_1)t} \\ & + i\Gamma_L \frac{(\omega_2 - \epsilon_R + i\delta_R)(\omega_1^* - \epsilon_R - i\delta_R)}{(\omega_1 - \omega_2)(\omega_1^* - \omega_2^*)(\omega_2 - \omega_2^*)} e^{i(\omega_2^* - \omega_2)t} \\ & + 2\Gamma_L\, \mathrm{Im}\left(\frac{(\omega_1^* - \epsilon_R - i\delta_R)(\omega_2 - \epsilon_R + i\delta_R)}{(\omega_1 - \omega_2)(\omega_1^* - \omega_2^*)(\omega_2 - \omega_1^*)} e^{(i\omega_0 - \bar{\Gamma}/2)t} \right), \end{aligned} \tag{25}$$

with the abbreviations $\bar{\Gamma} := \Gamma_L + 2\delta_R$ and $\epsilon := \epsilon_d - \epsilon_R$. The frequencies ω_1 and ω_2 are the poles of the spectral function $A(\omega)$ with negative imaginary part and ω_1^* and ω_2^* are its other two poles. The first part of $n(t)$ in Eq. (25) corresponds to the steady state. The next two lines describe how the system performs exponential decay toward this steady state because the exponents are real and negative. The last line of Eq. (25) is responsible for the oscillations because its exponent contains the imaginary part $i\omega_0 t$, which is given by

$$\begin{aligned} \omega_0 = \mathrm{Re}\Bigg\{ \Bigg[& (\epsilon_d + \varepsilon_R - i\bar{\Gamma}/2)^2 \\ & - 4(\varepsilon_R - i\delta_R)(\epsilon_d - i\Gamma_L/2) + 4\frac{\Gamma_{R,0}^2}{2\pi} \Bigg]^{1/2} \Bigg\}. \end{aligned} \tag{26}$$

If we switch off the coupling to the left side and the width on the right, i.e., $\Gamma_L \to 0$ and $\delta_R \to 0$, we recover the frequency $\omega_0 = \sqrt{\epsilon^2 + 4\frac{\Gamma_{R,0}^2}{2\pi}}$ of coherent oscillations in an isolated two-level system [remember the mapping to the double-dot model in Eq. (15)]. In Fig. 6, one recognizes that in the absence of the detuning $\epsilon_d - \varepsilon_R$, the frequency ω_0 completely vanishes with a nonanalyticity where $\delta_R/\Gamma_{R,0}$ is of the order of 1. This nonanalyticity appears when the radicand in Eq. (26) changes sign (at $\epsilon_d = \varepsilon_R$ it is purely real). When detuning is present, the frequency ω_0 does not completely vanish for $\delta_R \to \infty$, but the oscillations of $n_d(t)$ are damped with the rate $\bar{\Gamma}/2 = \delta_R + \Gamma_L/2$, such that in the Markovian limit $\delta_R \to \infty$, no oscillations survive.

V. CONCLUSIONS

The main message of this paper is that one must be careful with NMMEs. We know that what we have here called MMEs may lead to incorrect results when non-Markovian effects are strong. However, we have found that in the non-Markovian regime NMMEs can be worse than MMEs. On one hand, NMMEs can give quantitative errors such as what occur in Fig. 4. On the other hand, the positivity of the density matrix is not in general conserved, which can lead to unphysical results such as a negative Fano factor and occupation probability, as in Figs. 4 and 5. We emphasize that the failure of the NMME does not result from the evaluation techniques we have used[11] but instead from the way the Born approximation is performed in the derivation of Eq. (16). We do not want to discourage using of NMMEs in general, but each time they are applied one should reason carefully why one expects them to yield better results than MMEs.

We have tried the dynamical-coarse-graining method as an alternative approach, that is more sophisticated than the MME but still in Lindblad form. For the time-independent quantities I, F, and $n(t \to \infty)$, we have found no improvement in comparison to the MME. For the time-dependent occupation probability, however, DCG does yield better results, at least for small times. We expect a similar improvement for the frequency-dependent Fano factor.

For the model considered here, the condition $\frac{\Gamma_{R,0}}{\delta_R} \ll 1$ must be fulfilled to ensure a good quality of the three presented weak-coupling approximations. It is certainly interesting to explore higher-order corrections to the presented perturbative approximations. However, such extensions should be treated with caution since nice features, such as positivity, may be lost when higher orders are included.

ACKNOWLEDGMENTS

We would like to thank S. Gurvitz, C. López-Monís, U. Kleinekathöfer, and T. Novotný for helpful discussions. This work was supported by DFG under Grant No. BR 1528/5-1.

APPENDIX A: DERIVATION OF THE KERNEL

We decompose our Hamiltonian into the free part $H_0 = \epsilon_d d^\dagger d + \Sigma_{k,a} \epsilon_{ka} c_{ka}^\dagger c_{ka}$ and the coupling $V = \Sigma_{k,a}(t_{ka} d^\dagger c_{ka} + t_{ka}^* c_{ka}^\dagger d)$. This enables us to define the density matrix in the interaction picture $\tilde{\chi}(t)$. It obeys the Liouville–von Neumann equation

$$\dot{\tilde{\chi}}(t) = -i[\tilde{V}(t), \tilde{\chi}(t)], \tag{A1}$$

where $\tilde{V}(t) = e^{iH_0 t} V e^{-iH_0 t}$ is the interaction-picture version of the coupling. A tilde will mark the interaction picture in all following text. By iterating Eq. (A1) twice, we obtain

$$\dot{\tilde{\chi}}(t) = -i[\tilde{V}(t), \tilde{\chi}(0)] - \int_0^t dt' [\tilde{V}(t), [\tilde{V}(t'), \tilde{\chi}(t')]]. \tag{A2}$$

At this point, we perform the second-order weak-coupling approximation by replacing the full density matrix $\tilde{\chi}(t')$ by a tensor product of the reduced density matrix $\tilde{\rho}(t)$ and the bath density matrix R_0, which we assume to be constant in time (Born approximation). The partial trace over the first commutator in Eq. (A2) vanishes. To proceed, we resolve the coupling into system operators S_i and bath operators B_i such that

$$\tilde{V}(t) = \tilde{S}_1(t)\tilde{B}_1(t) + \tilde{B}_2(t)\tilde{S}_2(t), \tag{A3}$$

where

$$\tilde{S}_1(t) = \tilde{d}^\dagger(t), \quad \tilde{B}_1(t) = \sum_{k,a} t_{ka} \tilde{c}_{ka}(t),$$

$$\tilde{S}_2(t) = \tilde{d}(t), \quad \tilde{B}_2(t) = \sum_{k,a} t_{ka}^* \tilde{c}_{ka}^\dagger(t). \tag{A4}$$

In the calculation that follows, we find that the off-diagonal elements of $\tilde{\rho}(t)$ decouple from the diagonal ones. With this knowledge, we can choose the off diagonals to be zero and neglect them in the density matrix, which we can therefore consider as a vector with two entries:

$$\tilde{\rho}(t) = \tilde{\rho}_{00}(t) dd^\dagger + \tilde{\rho}_{11}(t) d^\dagger d = \begin{pmatrix} \tilde{\rho}_{00}(t) \\ \tilde{\rho}_{11}(t) \end{pmatrix}. \tag{A5}$$

To evaluate the double commutator in Eq. (A2) is lengthy but straight forward and yields

$$\dot{\tilde{\rho}}(t) = \int_0^t dt' \mathcal{W}(t-t') \tilde{\rho}(t') \tag{A6}$$

with

$$\mathcal{W}(t) = \begin{pmatrix} -\gamma_L(t) & \gamma_R(t) \\ \gamma_L(t) & -\gamma_R(t) \end{pmatrix}. \tag{A7}$$

For the entries of $\mathcal{W}(t)$, we need to explicitly perform traces over the reservoirs

$$\gamma_L(t) = e^{i\epsilon_d t} \operatorname{Tr}\{\tilde{B}_2(0)\tilde{B}_1(t)R_0\} + e^{-i\epsilon_d t} \operatorname{Tr}\{\tilde{B}_2(t)\tilde{B}_1(0)R_0\}. \tag{A8}$$

With infinite bias, i.e., $R_0 = \Sigma_k c_{kL}^\dagger c_{kL}$, this becomes

$$\gamma_L(t) = \sum_k |t_{kL}|^2 2\cos[(\epsilon_{kL} - \epsilon_d)t]$$

$$= 2\int_{-\infty}^{\infty} \frac{d\omega}{2\pi} \Gamma_L(\omega) \cos[(\omega - \epsilon_d)t]. \tag{A9}$$

In the same manner, we get

$$\gamma_R(t) = 2\int_{-\infty}^{\infty} \frac{d\omega}{2\pi} \Gamma_R(\omega) \cos[(\omega - \epsilon_d)t]. \tag{A10}$$

Physically, the upper right matrix element of $\mathcal{W}(t)$ describes a jump from the dot to the right lead. Thus, we can say that it increases the number of passed electrons by one while all other matrix elements leave it unchanged. Thus, we distinguish

$$\mathcal{W}_0(t) = \begin{pmatrix} -\gamma_L(t) & 0 \\ \gamma_L(t) & -\gamma_R(t) \end{pmatrix}, \tag{A11}$$

$$\mathcal{W}_1(t) = \begin{pmatrix} 0 & \gamma_R(t) \\ 0 & 0 \end{pmatrix}. \tag{A12}$$

APPENDIX B: EVALUATION OF CURRENT AND NOISE

We use a bra-ket-type notation, where the equilibrium state is represented by the ket

$$|0\rangle\rangle = \lim_{t\to\infty} \rho(t) = \frac{1}{\hat{\gamma}(0)} \begin{pmatrix} \hat{\gamma}_R(0) \\ \hat{\gamma}_L(0) \end{pmatrix}, \tag{B1}$$

that we obtain by setting $\dot{\rho}=0$ in Eq. (16). We define the bra

$$\langle\langle \tilde{0}| = (1,1), \tag{B2}$$

and construct the projector

$$\mathcal{P} = \mathcal{P}^2 = |0\rangle\rangle\langle\langle\tilde{0}| = \frac{1}{\hat{\gamma}(0)} \begin{pmatrix} \hat{\gamma}_R(0) & \hat{\gamma}_R(0) \\ \hat{\gamma}_L(0) & \hat{\gamma}_L(0) \end{pmatrix}, \tag{B3}$$

and the projector $\mathcal{Q} = \mathcal{Q}^2 = \hat{1} - \mathcal{P}$. The resolvent of the Laplace-transformed kernel from Eq. (19) is $\mathcal{R}(\Lambda, \chi, z) := \mathcal{Q}[\mathcal{W}(\chi, z) - \Lambda \cdot 1]^{-1}\mathcal{Q}$. We only need its value at zero, $\mathcal{R} := \mathcal{R}(0,0,0)$, which is

$$\mathcal{R} = \frac{1}{[\hat{\gamma}_L(0) + \hat{\gamma}_R(0)]^2} \begin{pmatrix} -\hat{\gamma}_L(0) & \hat{\gamma}_R(0) \\ \hat{\gamma}_L(0) & -\hat{\gamma}_R(0) \end{pmatrix}. \tag{B4}$$

We introduce the coefficients of the kernel's Taylor series via

$$\mathcal{W}(\chi, z) = \overline{\mathcal{W}} + \overline{\mathcal{W}}'\chi + \dot{\overline{\mathcal{W}}} z + \frac{1}{2}(\overline{\mathcal{W}}'\chi^2 + 2\dot{\overline{\mathcal{W}}}'\chi z + \ddot{\overline{\mathcal{W}}} z^2) + \cdots. \tag{B5}$$

The expressions for current and the zero-frequency noise[11,44] are now obtained as

$$I = e\langle\langle \tilde{0}|\overline{\mathcal{W}}'|0\rangle\rangle/i,$$

$$S = e^2[\langle\langle \tilde{0}|\overline{\mathcal{W}}''|0\rangle\rangle - 2\langle\langle \tilde{0}|\overline{\mathcal{W}}'\mathcal{R}\overline{\mathcal{W}}'|0\rangle\rangle]/i^2$$

$$- 2ie[\langle\langle \tilde{0}|\dot{\overline{\mathcal{W}}}'|0\rangle\rangle - \langle\langle \tilde{0}|\overline{\mathcal{W}}'\mathcal{R}\dot{\overline{\mathcal{W}}}|0\rangle\rangle]. \tag{B6}$$

Performing the derivatives and matrix multiplications leads to the results of Eq. (21).

*zedler@physik.tu-berlin.de

[1] Y. M. Blanter and M. Büttiker, Phys. Rep. **336**, 1 (2000).
[2] *Quantum Noise in Mesoscopic Physics*, edited by Y. V. Nazarov (Kluwer Academic, Dordrecht, 2003).
[3] Y. Blanter, arXiv:cond-mat/0511478 (unpublished).
[4] G. Kießlich, E. Schöll, T. Brandes, F. Hohls, and R. J. Haug, Phys. Rev. Lett. **99**, 206602 (2007).
[5] A. Braggio, C. Flindt, and T. Novotný, Physica E (Amsterdam) **40**, 1745 (2008).
[6] A. Braggio, J. König, and R. Fazio, Phys. Rev. Lett. **96**, 026805 (2006).
[7] I. Knezevic, Phys. Rev. B **77**, 125301 (2008).
[8] R. Aguado and T. Brandes, Phys. Rev. Lett. **92**, 206601 (2004).
[9] T. Brandes, Phys. Rep. **408**, 315 (2005).
[10] Y. N. Chen and G. Y. Chen, Phys. Rev. B **77**, 035312 (2008).
[11] C. Flindt, T. Novotný, A. Braggio, M. Sassetti, and A.-P. Jauho, Phys. Rev. Lett. **100**, 150601 (2008).
[12] S. Datta, *Electronic Transport in Mesoscopic Systems* (Cambridge University Press, Cambridge, 1995).
[13] S. Datta, *Quantum Transport: Atom to Transistor* (Cambridge University Press, Cambridge, 2005).
[14] H. Haug and A.-P. Jauho, *Quantum Kinetics in Transport and Optics of Semiconductors* (Springer-Verlag, Berlin, 2007).
[15] H.-P. Breuer and F. Petruccione, *The Theory of Open Quantum Systems* (Clarendon Press, Oxford, 2006).
[16] M. Nedjalkov, H. Kosina, S. Selberherr, C. Ringhofer, and D. K. Ferry, Phys. Rev. B **70**, 115319 (2004).
[17] M. Nedjalkov, D. Vasileska, D. K. Ferry, C. Jacoboni, C. Ringhofer, I. Dimov, and V. Palankovski, Phys. Rev. B **74**, 035311 (2006).
[18] D. Querlioz, J. Saint-Martin, A. Bournel, and P. Dollfus, Phys. Rev. B **78**, 165306 (2008).
[19] T. H. Stoof and Y. V. Nazarov, Phys. Rev. B **53**, 1050 (1996).
[20] S. A. Gurvitz and Y. S. Prager, Phys. Rev. B **53**, 15932 (1996).
[21] F. Kaiser, M. Strass, S. Kohler, and P. Hänggi, Chem. Phys. **322**, 193 (2006).
[22] A. Thielmann, M. H. Hettler, J. König, and G. Schön, Phys. Rev. Lett. **95**, 146806 (2005).
[23] X. Q. Li, J. Luo, Y. G. Yang, P. Cui, and Y. J. Yan, Phys. Rev. B **71**, 205304 (2005).
[24] J. N. Pedersen and A. Wacker, Phys. Rev. B **72**, 195330 (2005).
[25] B. Elattari and S. A. Gurvitz, Phys. Rev. A **62**, 032102 (2000).
[26] Matisse W. Y. Tu and W.-M. Zhang, Phys. Rev. B **78**, 235311 (2008).
[27] M. Thorwart, E. Paladino, and M. Grifoni, Chem. Phys. **296**, 333 (2004).
[28] P. Huang and H. Zheng, J. Phys. (Paris), Colloq. **20**, 395233 (2008).
[29] U. Kleinekathöfer, J. Chem. Phys. **121**, 2505 (2004).
[30] P. W. Anderson, Phys. Rev. **124**, 41 (1961).
[31] U. Fano, Phys. Rev. **124**, 1866 (1961).
[32] G. D. Mahan, *Many-Particle Physics* (Springer, Netherlands, 2000).
[33] H. Bruus and K. Flensberg, *Many-Body Quantum Theory in Condensed Matter Physics* (Oxford University Press, Oxford, 2004).
[34] A. C. Hewson, *The Kondo Problem to Heavy Fermions* (Cambridge University Press, Cambridge, 1993).
[35] A. D. Stone and P. A. Lee, Phys. Rev. Lett. **54**, 1196 (1985).
[36] M. Cini, Phys. Rev. B **22**, 5887 (1980).
[37] G. Stefanucci and C.-O. Almbladh, Phys. Rev. B **69**, 195318 (2004).
[38] G. Schaller, P. Zedler, and T. Brandes, Phys. Rev. A **79**, 032110 (2009).
[39] M. Y. Sumetskii and M. Fel'shtyn, JETP Lett. **53**, 24 (1991).
[40] L. S. Levitov and G. B. Lesovik, JETP Lett. **58**, 230 (1993).
[41] H. Lee, L. S. Levitov, and A. Y. Yakovets, Phys. Rev. B **51**, 4079 (1995).
[42] B. Elattari and S. A. Gurvitz, Phys. Lett. A **292**, 289 (2002).
[43] G. Kießlich, P. Samuelsson, A. Wacker, and E. Schöll, Phys. Rev. B **73**, 033312 (2006).
[44] C. Flindt, A. Braggio, and T. Novotný, AIP Conf. Proc. **922**, 531 (2007).
[45] A. Braggio, C. Flindt, and T. Novotný, J. Stat. Mech.: Theory Exp. (2009) P01048.
[46] D. Urban and J. König, Phys. Rev. B **79**, 165319 (2009).
[47] G. Lindblad, Commun. Math. Phys. **48**, 119 (1976).
[48] G. Schaller and T. Brandes, Phys. Rev. A **78**, 022106 (2008).
[49] D. A. Lidar, Z. Bihary, and K. B. Whaley, Chem. Phys. **268**, 35 (2001).